

# Performance Enhancement of PA-TFC RO Membrane by Using Magnesium Silicate Nanoparticles

Yousra H. Kotp<sup>1</sup> · Yehia A. Shebl<sup>2</sup> · Mohamed S. El-Deab<sup>2</sup> · Bahgat E. El-Anadouli<sup>2</sup> · Hosam A. Shawky<sup>1</sup>

Received: 1 August 2017 / Accepted: 28 August 2017  
© Springer Science+Business Media, LLC 2017

**Abstract** This study focuses on to the change of the execution of polyamide (PA) thin-film composite (TFC) reverse osmosis (RO) membrane utilizing surface alteration by MgSiO<sub>3</sub> nanoparticles. This has been an expert by means of holding of the practical grafting of PA layer with magnesium silicate nanoparticles (MgSiO<sub>3</sub>) in the presence of 2-acylamido 2-methyl propane sulphonic acid (AMPS) as condensing monomer. To confirm the presence of MgSiO<sub>3</sub> nanoparticles and to inspect the morphology of the TFC nanoparticles layer SEM, FT-IR, XRD, TGA and DMA analysis were used. The outcomes demonstrated that the AMPS are effectively joined on the TFC film surface with an upgrade in thermal and mechanical decencies contrasted with pristine TFC layer. Besides, the contact angle estimations demonstrate an increase in the hydrophilicity of the thin film surface by the addition of nanoparticles. The water flux and salt rejection of the modified membranes were 25 L/m<sup>2</sup> h and 95.5%, respectively.

**Keywords** Reverse osmosis · Water desalination · Thin film composite · Magnesium silicate · Nanomaterials

## 1 Introduction

Water requirements are continually growing up as a direct result of inhabitation increase (The ask for water has

developed, twice as quick as population) [1], also enhancing ways of life besides that the governments put regulates and policies to develop and promote industrialization, adjacent to that the environmental changes impact also the current natural freshwater shortage, where numerous areas on the planet don't have simple access to drinkable water, particularly, in the Middle East district and North Africa (MENA), a definitive water-rare zone of the world [2].

Egypt, for example, has entered a state where its national economic development is under a significant negative stress as the deficiency of the available freshwater sources. Egypt has already reached a sign of scarcity where the threshold rate is about (1000 m<sup>3</sup>/capita/year) in the nineties. As a limit of absolute shortage (500 m<sup>3</sup>/ca/year) is utilized, this will be clear with populace forecast for 2025 which will take Egypt down to 500 m<sup>3</sup>/ca/year [3].

Desalination nowadays considered as an essential and sustainable source of water for numerous worldwide countries that supply a safe and extreme source of drinkable and fresh water particularly in the coastal districts, where, around 23% of the total populace exist within about 100 km of the sea, also populace quantity in these regions is greater than triple the universal rate [4].

Water desalination has the ability to get fresh water from various kinds of water sources that without desalination not to be fit for different human uses. Water desalination has a several proven and fixed technologies which supply the water for the population in regions those have insufficient fresh water sources or to furnish ultra pure water for the industrial process [5]. Currently, it is assessed that there are more than 18,000 desalination plants in the service in more than 150 nations around the globe produce a total capacity up to 86.5 million cubic meters per day; a great portion of them in the Middle East and the quantity is continuously growing. Membrane technology shared about 70% of the

✉ Yousra H. Kotp  
yoso20002000@yahoo.com

<sup>1</sup> Egyptian Desalination Research Center of Excellence (EDRC), Desert Research Center, P.O.B 11753, Cairo, Egypt

<sup>2</sup> Chemistry Department, Faculty of Science, Cairo University, P.O.B 12613, Giza, Egypt

total capacity of global desalted water and about 65% of them are RO membrane separation plants while about only 28% is thermal desalination plants [6]. Commercial interest in Reverse Osmosis technology and the rate of installed RO desalination stations has been expanding steadily over the recent 10 years due to continuous process improvements, mainly the striking advances in the membrane properties, the great development of the energy recovery devices efficiency, also improvements in the module layout, process design, and feed pretreatment resulting in the huge decline in overall water production costs [7].

Execute a balance between increased productivity as well as increase the rate of the salt rejection or even maintain it without Loss, will continue the main driver to improve RO membranes, also It was proven that increase the productivity of the membrane can reduce the price of desalinated water, even if accompanied by a little decrease in salt rejection rates [8].

Uses of nanotechnology could offer remarkable development and improvement to water treatment process, also offer significant solutions for current and future freshwater demands, additionally, provide favorable solutions for water quality challenges. Now, desalination membranes set up on the use of nanomaterials are realistic available, with others either close market start or in the methodology of being advanced [9]. Beginning tests recommended that the novel membrane layers have doubled the permeate water, or lower the consumed power to half, and shortening the aggregate cost of desalinated water by as a considerable measure as 25% [10].

Incorporation of a functional nanomaterial inside the layers of the polymer membrane for the manufacture of which was agreed to be called Mixed Matrix membrane that consisting of an inorganic filler (with excellent thermal, biological and chemical stabilities) like zeolite, metal oxide, carbon nanotubes, silver, silica nanoparticles dispersed in the continuous thin polymeric phase (with high-performance flexibility and processability properties) through the interfacial polymerization process, has been Used widely to offers a great possibility to enhance permeability, fouling resistance, also mechanical and thermal stability of the desalination membrane [11].

One of the key parameters for the effective execution of nanocomposite MMMs is to enhance the scattering of inorganic nanomaterial fillers in polymer lattice through the foundation of particular and strong synergy between the nanofiller and the polymer matrix [12]. Zehhaf and co-workers used Algerian natural montmorillonites for the removal of arsenic(III) from aqueous solution and the results suggest that Algerian natural montmorillonites could be used as low-cost and effective filtering materials for removal of arsenic from water [13]. Perversely, the weak interfacial adaptability of the dispersed nano filler through the polymer leads to

nano filler agglomeration, which gives rise to the development of unintended voids in the membranes, and therefore nanofiller may be leached especially after a period of operation and susceptible to long term of the required operating pressure and also the cleaning process of the membrane. This eventually leads to hindered membrane properties and its lifetime, add to that health risks and environmental hazards of the discharged nonmaterial [14]. Among various ways to produce MMMs, it can be fabricated by covering or placing an inorganic layer above the formed PA membrane surface, as this PA active thin layer highly sensitive and can easily be damaged by various physical and chemical issues, so using a coating inorganic layer with superior resistance to chemical and physical attack and more thermal stability, cannot just enhance the PA membrane properties but also may be added a new characters to the membrane colligative properties. so here in this study, we development of a MMM by making a surface modification via attachment of inorganic nanoparticles like magnesium silicate nanoparticles ( $\text{MgSiO}_3\text{NPs}$ ) as a coating layer covering a routine TFC membrane to couple the two different properties of organic and inorganic substances like high processability of and high activity of organic polymers, as far as brilliant thermal and chemical stabilities, high selectivity and high permeability, of inorganic materials.

In this work  $\text{MgSiO}_3\text{NPs}$  incorporated with 2-acrylamido-2-methylepropane sulfonic acid (AMPS) grafting solution was successfully synthesized using the redox grafting technique, perfecting surface coating with nanoparticles and enhance the application of PA(TFC) membranes. The chemical structure and the morphology of the membrane grafted and modified with nanoparticles were studied and characterized by/ X-ray diffraction (X-ray), infrared spectroscopy (FTIR), Scanning electron microscope (SEM), thermal analysis (TGA), assessments of mechanical property, and contact angle (CA) determination. Optimization of the amount of  $\text{MgSiO}_3\text{NPs}$  incorporated onto the TFC surface was proposed leading to the best RO membrane performance.

## 2 Experimental

### 2.1 Materials

Polysulfone pellets Udel P-3500 were provided by Solvay advanced polymer, USA, N,N-dimethylacetamide (DMA) were supplied from (Sigma-Aldrich). metaphenylenediamine (MPDA), trimesoyl chloride (TMC), triethyl amine (TEA), (+)-10-champhor sulfonic acid (CSA), sodium lauryl sulfate (SLS), 2-acrylamido-2-methyl propane sulfonic acid (AMPS), potassium persulfate  $\geq 99.0\%$ , sodium metabisulfite  $\geq 99.0\%$ , and a commercial form of nano-magnesium silicate ( $\text{MgSiO}_3$ ) (diameter of particles about 15 nm)

was afforded from Dixiang Chemical Engineering Co., Ltd. (Shanghai, China). Other reagents such as *n*-hexane, sodium chloride (NaCl) are of analytical grade, and pure water with the conductivity less than 5  $\mu\text{s}/\text{cm}$  was produced by a two-stage reverse osmosis system.

## 2.2 Characterization of MgSiO<sub>3</sub> NPs

Scanning electron microscope (*SEM Model Quanta FEG*) connected with EDX Unit, with speeding up voltage 30 kV, magnification 250 $\times$  up to 20,000 $\times$  and resolution for gun 1 m also XRD analysis utilizing (*Shimadzu X-ray*) diffractometer, (*Model XD 490 Shimadzu, Kyoto, Japan*) and FTR-IR analysis (*Nicolet avatar 230 spectrometers*) at room temperature were used to characterize the morphology of MgSiO<sub>3</sub> NPs.

## 2.3 Preparation of Microporous Polysulfone Support Membrane

PS casting solution was prepared by melting 15 wt% PSF in DMA at 80–90 °C with continuous stirring. The resultant polysulfone solution was molded onto a glass tray and coagulates in a water bath. After 10 min of gelation, the resulting PSF membrane was removed from the gelation bath and washed with bidistilled water to remove the residual DMA. The prepared PSF support membrane was saved in distilled water for at minimal 24 h before use. The membrane was then posterior utilized as a support milieu for TFC membrane production.

## 2.4 Manufacture of Thin Film Composite Membranes

Thin film coating was synthetic/fabricated to deposit the active thin layer of polyamide (PA) over the porous PSF bolster membrane. Aromatic polyamide TFC RO membranes were synthesized by the interfacial polymerization of MPD (2.0 wt%) in aqueous phase and Trimethylol chloride (0.15 wt%) in organic phase (*n*-hexane), CSA (4.0 wt%), SLS (0.15 wt%), and TEA (3 wt%), were combined into the aqueous phase. CSA and SLS were used to improve the absorption of MPD in microporous polysulfone support membrane. TEA hurried the MPD–TMC reaction by eliminating hydrogen halide created during amide bond formation [15]. Firstly, the support membrane was soaked with MPD solution for 2 min. The overabundance solution was removed by a rubber roller. Then the support membrane covered with 0.15 wt% of TMC-hexane solution for the 60 s, followed by rinsing with *n*-hexane and cured at 80 °C for 10 min. This resulted in the creation of ultra-thin aromatic polyamide film over the support membrane that was denoted as “parent membrane” in this work. The membranes then washed and

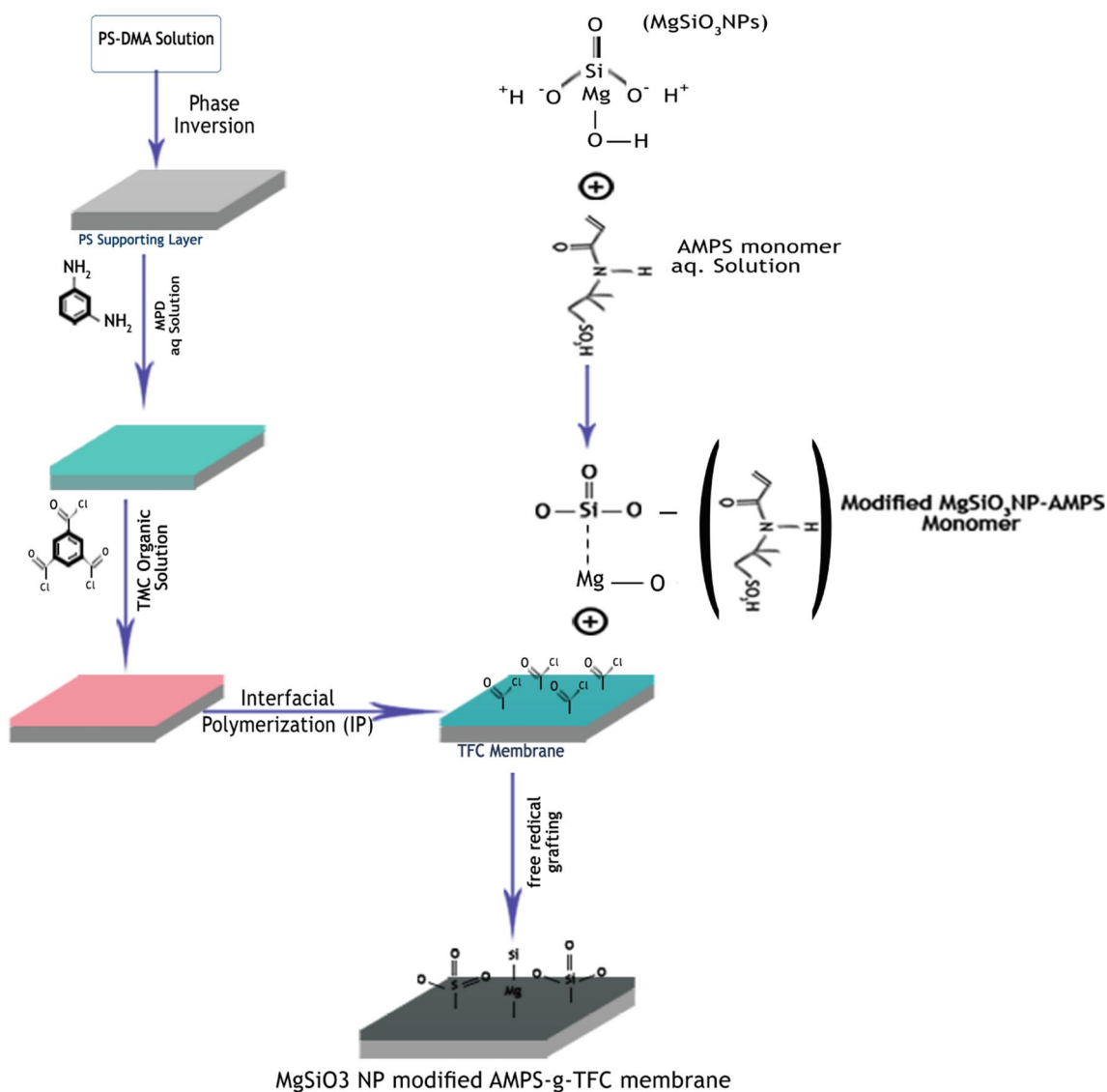
preserved in deionized water before characterization tests or application studies.

## 2.5 Fabrication of MgSiO<sub>3</sub> NPs Modified AMPS-g-TFC Membranes

Firstly redox grafting was performed utilizing a blend of redox initiators consisting of potassium persulfate K<sub>2</sub>S<sub>2</sub>O<sub>8</sub> (2% of monomers) and sodium metabisulfite Na<sub>2</sub>S<sub>2</sub>O<sub>5</sub> (1/3 of K<sub>2</sub>S<sub>2</sub>O<sub>8</sub>) on a newly fabricated TFC flat sheet membrane for about 20 min. Secondly a different mixture of various concentrations of (AMPS) monomer (2.5–15%) and (MgSiO<sub>3</sub>) nanoparticles (0.005–0.1% of monomer concentration) were sonicated for 1 h, then added to the above initiated TFC flat sheet membrane, and immediately put in the oven to complete the reaction at varied temperatures and different times (Scheme 1).

## 2.6 Membrane Characterization

Membranes used for chemical and morphological examination are rinsed with DI water and dehydrated before characterization. The thin film composite RO membrane surface was characterized by Fourier transform infrared (FT-IR) made with a (*Nicolet avatar 230 spectrometers*) at room temperature. Irtran crystal at a 45° angle of downfall employed for FT-IR analysis of different samples. Scanning electron microscopy (SEM) with (*SEM Model Quanta FEG*) connected with EDX Unit, with speeding up voltage 30 kV, magnification 250 $\times$  up to 20,000 $\times$  and resolution for gun 1 m was used for examination of membrane morphology. Samples are coated with gold. X-ray diffraction patterns were performed utilizing (*Shimadzu X-ray*) diffractometer, (*Model XD 490 Shimadzu, Kyoto, Japan*) with a nickel filter and Cu K $\alpha$  radiation tube. Thermal stability and water content of the fabricated membranes were done using a (*Shimadzu DT-60H thermal analyzer, Shimadzu, Kyoto, Japan*). The films measured from 25 to 1000 °C with a warming rate equal to 15°/min. Dynamic Mechanical Analysis (DMA) mechanical proprieties where tensile strength and elongation of membranes were determined by a universal mechanical testing instrument (*DMATAQ800*) (Film tension clamp) of different membranes under study. Measurements were executed at room temperature and a strain rate of 50 mm min<sup>-1</sup> was utilized. For all membrane, at minimum three-unit tests were examined. Also, the surface hydrophilicity of the films was particulate by the estimation of the water contact edge with a contact point goniometer from (VCA Video Contact Angle System, Kr ÜssDSA25B, Germany) at room temperature, at least, six estimations at various locales were procured for each layer.



**Scheme 1** Schematic diagram of grafting MgSiO<sub>3</sub> NP-AMPS modified monomer onto the surface of PA TFC membrane

## 2.7 Performance Test

ALFA LAVAL pilot-scale laboratory unit for membrane filtration (*Model LabUnit M20*) was used for testing the performance of synthesized reverse osmosis membranes (Fig. 1). Flat sheet layers with a viable region of 0.018 m<sup>2</sup> were set in the test instrument with the polyamide dynamic layer confronting the bolster water. All film tests were carried and tried at minimum twice with a sum of three layers tests for RO execution, the normal outcomes were taken, the volume of penetrating was taken in 1 h and the flux communicated regarding (L/m<sup>2</sup> h). The standard conductivity meter was utilized to assess the salt fixations in the nourish and the pervade water for setting film effectiveness as given below:

$$\text{Salt Rejection (\%)} = 1 - C_p/C_f \times 100 \quad (1)$$

where  $C_f$  and  $C_p$  are the concentration of salts in the feed water and in permeate flux, respectively.

## 3 Results and Discussion

### 3.1 MgSiO<sub>3</sub> NPs Characteristics

It was clear from SEM image in Fig. 2, MgSiO<sub>3</sub> NPs are well distributed, of spherical morphology and of very small and highly agglomerated particles with the rounded shape. The functional groups of the MgSiO<sub>3</sub> NPs were resolved using the FTIR spectrum as presented in Fig. 3. A

**Fig. 1** Schematic diagram for LabUnit M 20 pilot-scale membrane filtration

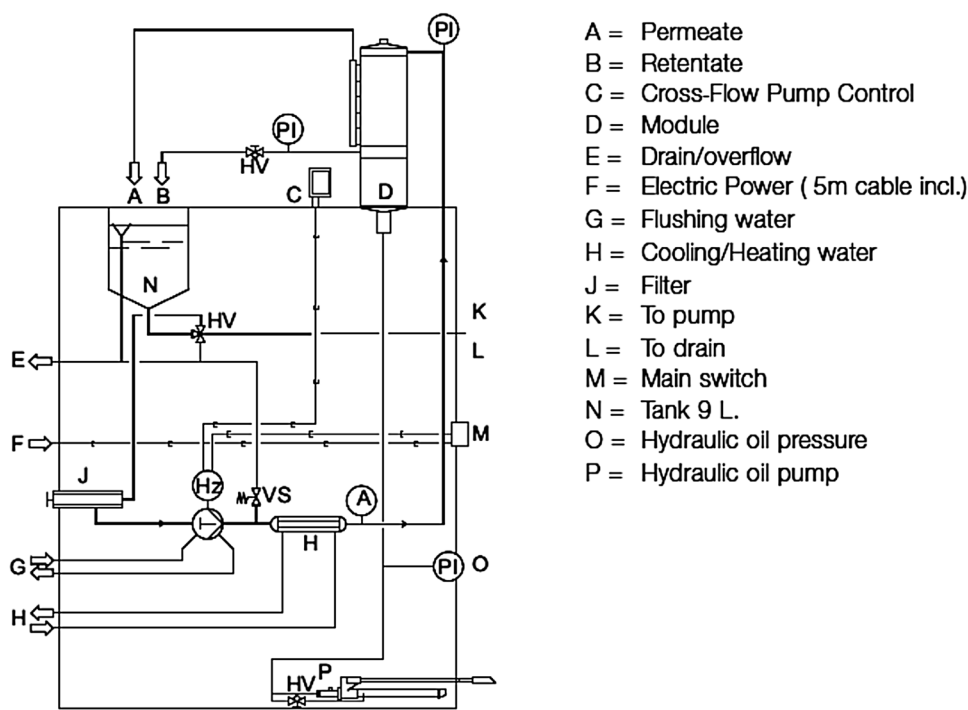
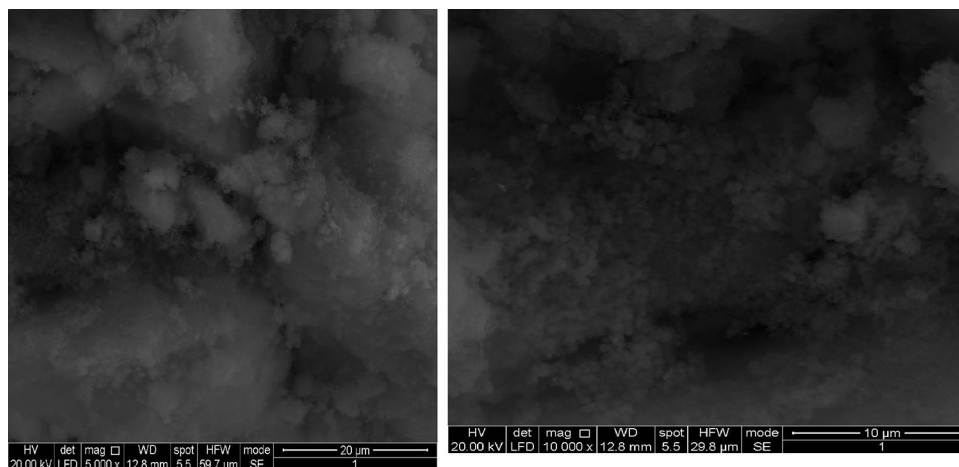


**Fig. 2** SEM images of magnesium silicate nanoparticles



peak at  $3697\text{ cm}^{-1}$  is characteristic to Mg–OH stretching, broadening peak near  $3437\text{ cm}^{-1}$  attributable to H-bonding of coordinated water and the strong peak at  $1017\text{ cm}^{-1}$  with a shoulder band at  $878\text{ cm}^{-1}$  is due to the existence of Si–O stretching vibrations, while the Mg–O vibrations occur at  $462\text{ cm}^{-1}$  [16, 17], which are remissible  $\nu$  Si–O,  $\nu$  Si–O–Mg and  $\nu$  Mg–O peaks with a slight shifting as in activated Montmorillonites [18]. X-ray diffraction displays crystalline structures (Fig. 4), where, three minor peaks demonstrate that the materials have identical patterns of crystalline nature. Also, the three minor peaks evidenced at  $18^\circ$ – $38^\circ$ ,  $51^\circ$  and  $58^\circ$ – $62^\circ$   $2\theta$  were pointed out to MgSiO<sub>3</sub> NPs.

### 3.2 Spectroscopic Characterizations of PSF, TFC, AMPS-g-TFC and MgSiO<sub>3</sub> NPs Modified AMPS-g-TFC Membranes

FTIR was performed to describe the successful preparation of TFC membranes onto the PSF support layer, to verify the successful graft polymerizations of AMPS onto TFC membranes, and to determine the functional groups in the MgSiO<sub>3</sub> NPs modified AMPS-g-TFC membrane. Figure 5, shows the characteristic peaks of PSF support layer and shows bands at  $737.1$ ,  $851.9$ ,  $1013$ ,  $1151.78$ ,  $1484$  and  $1579\text{ cm}^{-1}$  corresponding to (aromatic hydrogen), isolated aromatic hydrogen, an ether group, a sulfonic group, alkane groups and C–H aromatics respectively [19, 20]. While/

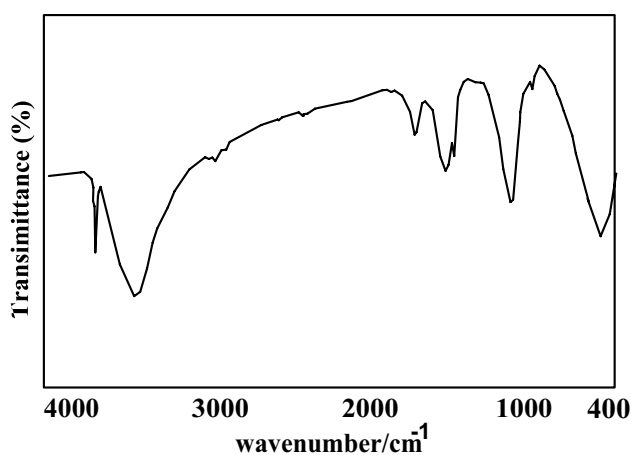


Fig. 3 ATR-FTIR spectra magnesium silicate nanoparticles

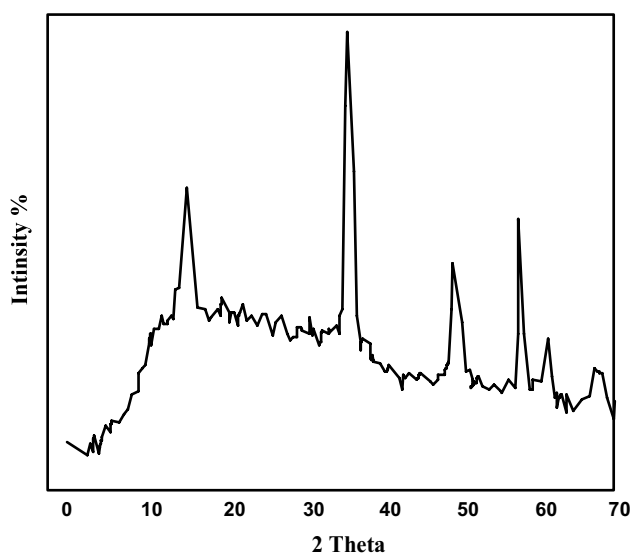


Fig. 4 XRD images of magnesium silicate nanoparticles

in the TFC membrane Fig. 5 elucidate different new peak bands appeared indicating the coating of PA barrier layer onto the PSF support layer. Two peak bands appear around 1597 and 1248  $\text{cm}^{-1}$  for the C=O stretching vibration and C–N group of the amide II on TFC membrane, respectively [21]. The spectrum reveals that there is a strong band around 1675.8  $\text{cm}^{-1}$ , which is characteristic of the C=O band of an amide group (amide I). Also, a small peak at 1777.09  $\text{cm}^{-1}$  which corresponded to C=O stretching (acid). The stretching peak at 3341–3473  $\text{cm}^{-1}$  can be assigned to N–H and O–H which overlapped together [22, 23]. The FTIR spectra of the AMPS-g-TFC membranes appeared in Fig. 5, where also the  $\text{NH}_2$  and C=O bands for TFC membrane, we observe specific absorption peak of AMPS monomer at 1294  $\text{cm}^{-1}$  because of the S–O group in the sulfonic acid ( $\text{SO}_2$ ) asymmetric and at 1152  $\text{cm}^{-1}$  due to asymmetric bands of

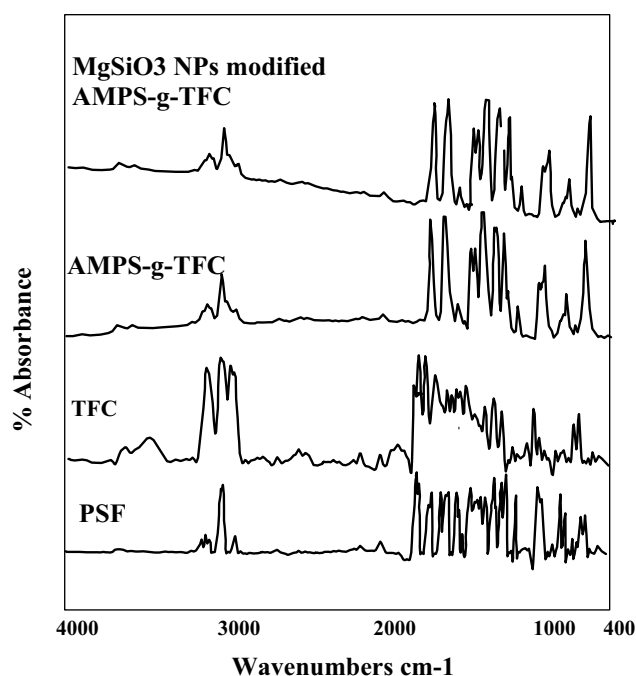


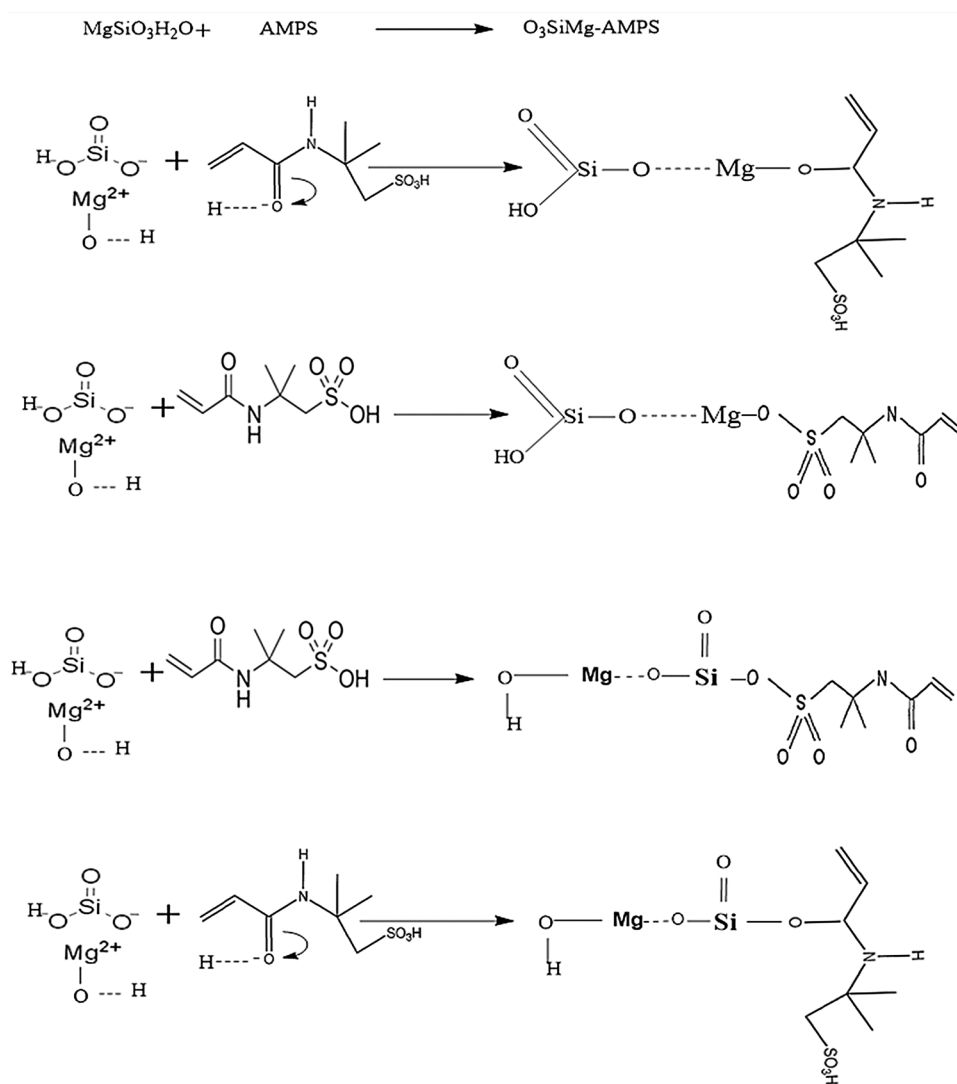
Fig. 5 ATR-FTIR spectra of polysulfone (PSF) support layer, thin film composite membrane (TFC), AMPS-g-TFC membrane, and  $\text{MgSiO}_3$ NPs modified AMPS-g-TFC membrane

(S–O) both referred by [23], who state 1250–1150 and 1100–1000  $\text{cm}^{-1}$ , respectively. The stretching band of OH group for sulfonic acid resemble at 3000  $\text{cm}^{-1}$ . As showed in Scheme 1, the specific absorption peak at ( $\sim 1654 \text{ cm}^{-1}$ ) resulted from the stretching vibration of C=O of the amide ( $-\text{CONH}_2$ ) group, this descending in the frequency peak of the carbonyl group because of the hydrogen bonds developed with N–H groups at the probable grafting position on the surface of TFC membrane [24].

Add to that the bands of –OH and –NH has been overlapped together to form a broad band between  $\sim 3161$  and 3892  $\text{cm}^{-1}$  this overlapping accompanied by a stretching vibration and collapse of –OH and –NH because of the construction of AMPS-g-TFC compound II, (Scheme 2) Also, the distinct peak at 1081  $\text{cm}^{-1}$  is an outcome of the behavior of S=O stretching in  $-\text{SO}_3$  of AMPS. Additionally, the peaks exhibit at the range from  $\sim 2970$  to  $\sim 3064 \text{ cm}^{-1}$  resembles C–H stretching vibrations of  $-\text{CH}_3$  and  $-\text{CH}_2$ , of AMPS [25].

By examine the  $\text{MgSiO}_3$  NPs modified AMPS-g-TFC membrane spectrum and match it with the primary TFC membrane as presented in the Fig. 5, it illustrated the existing of the new specific stretching band with 1904  $\text{cm}^{-1}$  as a result of Si–O stretching vibrations for  $\text{MgSiO}_3$  NPs [26]. The spectra also showed a wideband around 3600  $\text{cm}^{-1}$  which represent an intermolecular hydrogen bond established by the covalent connection of the carbonyl Oxygen

**Scheme 2** Four expected mechanisms of the reaction and bonds formed between  $\text{MgSiO}_3$  NPs and AMPS monomer to give  $\text{MgSiO}_3$  NP-AMPS modified monomer which has been grafted on PA TFC membrane surface by free radical grafting technique



of AMPS to the hydroxyl group associated with  $\text{MgSiO}_3$  NPs [27], as the appearing of the peak at about  $3900\text{ cm}^{-1}$  is may be attributed to silica-water interaction of Si-OH vibration style [28]. So as a result of adding  $\text{MgSiO}_3$  NPs to the AMPS grafting solution leading to shifting the C=O stretching vibrational peak due to delocalization of electrons distribution across the unsaturated system which stabilizes it by lowering its energy in the presence of electron donated from the Mg atoms this aspect agrees with the hypothesis revealed in the literature [18, 29]. conclusively, these peaks suggest the succeeded combination of  $\text{MgSiO}_3$  NPs with AMPS grafting monomer as a surface coating of TFC membrane.

Investigation of surface nature of the PSF and the TFC membranes and illustration the difference in the structure pattern between the AMPS-g-TFC and  $\text{MgSiO}_3$  NPs modified AMPS-g-TFC and that may take place during grafting with the AMPS, as well as after combination of the  $\text{MgSiO}_3$  NPs into the TFC membrane were done by X-ray diffraction

(XRD) technique. In Fig. 6, the typical diffraction peak for pure PSF is recognized at a  $2\theta$  value of 18.00. The spectrum exhibited the highly amorphous character of PSF [30]. The broad peak at 18.00 ( $2\theta$ ) resembled with low crystallinity, while the X-ray diffraction peak of TFC membrane appears at a  $2\theta$  value of 18.01. Also, the presence of wide curves with moderate intensity centered on 18 of  $2\theta$  of TFC, which indicate the presence of semi-crystalline nature concerning to the composite membrane [31]. In addition to the crystalline part in the TFC is a result to the polyamide surface layer and the amorphous zone is due to PSF support layer. The broad peak center on every X-ray formula was referred to the average inter-segmental distance of polymer main chains [32]. Figure 6, reports the XRD pattern of AMPS-g-TFC membranes which are crystalline in nature and give three crystalline peaks at  $2\theta$  angles of 26.2, 38.1 and 44.4 with the union of the dispersal peak concerning amorphous PS, nevertheless mean that their position is moderately shifted

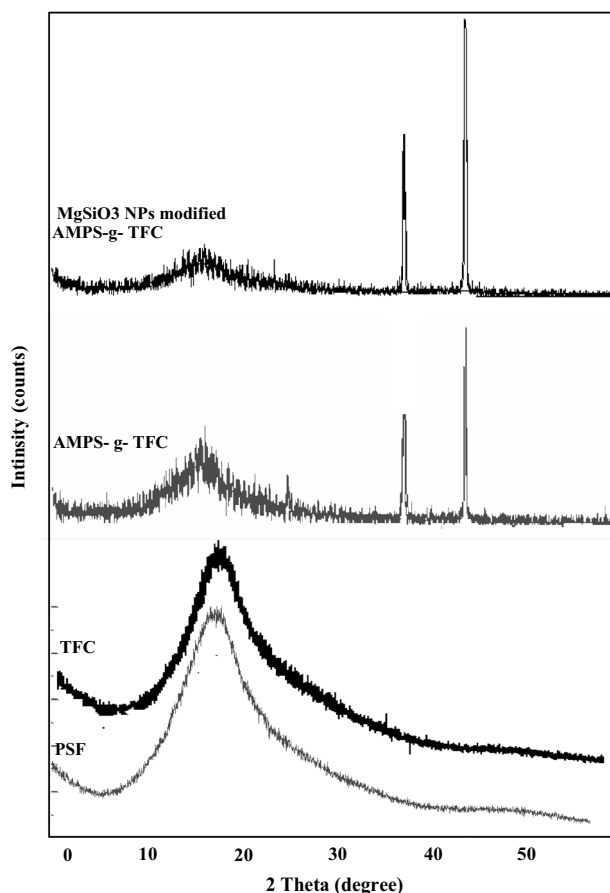


**Fig. 6** XRD images of polysulfone (PSF) support layer, thin film composite membrane (TFC), AMPS-g-TFC membrane, and MgSiO<sub>3</sub> NPs modified AMMPS-g-TFC membrane

[33]. The MgSiO<sub>3</sub>NPs modified AMPS-g-TFC membrane displays six crystalline specific peaks beside that the main fundamental peaks of MgSiO<sub>3</sub> NPs with values of 2 equal 10.2, 17.80, 18.31, 38.1, 44.4 and 54.6. The XRD pattern explains that MgSiO<sub>3</sub> NPs successfully integrated into the grafted layer above the pristine membrane surface, but, it is noted that, characteristic peaks related to the grafted

layer were displaced to in significantly lower angles when correlated with the MgSiO<sub>3</sub> NPs peaks. This change may be explained by the synergy between MgSiO<sub>3</sub>NPs and the AMPS through the modified grafting monomer preparation. Table 1 detects the comparison in terms of peak position relative intensity FWHM and d space in the AMPS-g-TFC and MgSiO<sub>3</sub>NPs modified AMPS-g-TFC membranes.

### 3.3 Microscopic Characterizations of the PSF Support Layer, PSF/TFC, and TFNC Membrane

As the surface morphology have a significant contribution to the resulted membrane performance The surface layer structures of PSF, TFC, AMPS-g-TFC, and MgSiO<sub>3</sub>NPs modified AMPS g TFC membranes were distinguished by SEM as displayed in Fig. 7. Figure 7a presents the PSF layer is highly porous with such as a finger like macro voids spongy–structure which can sustain high pressure [34]. Also, TFC membrane was examined by SEM as from Fig. 7b we can observe very thin surface layer is rough and dense with a well formed “ridge and valley” asymmetric structure which is representative for a typical PA membrane [35]. Figure 7c shows that the attachment of the grafted monomer onto the active polyamide surface was accompanied by an expansion in surface roughness and nodular morphology related to unchanged one. From SEM image in Fig. 7d we can observe the presence of MgSiO<sub>3</sub>NPs nanoparticles within the grafted layer which leads to more advancing in membrane surfaces roughness morphology also increasing not only in pore density but also in the size. We can suppose that the incorporation of MgSiO<sub>3</sub>NPs enhance the features of the membrane surface and create new stream channels through the thin layer making a direct impact on membrane water permeability Additionally the cross sectional SEM images of AMPS-g-TFC and MgSiO<sub>3</sub> NPs modified AMPS-g-TFC membranes appeared in Fig. 8a, b which shows that the surface modification achieved by this study results in a small increase in the thickness of the resulted membrane correlated to initial TFC membrane.

**Table 1** XRD data of AMPS-g-TFC and MgSiO<sub>3</sub> NPs modified AMPS-g-TFC membranes

Membrane type	Pos. [2θ]	d-spacing [Å <sup>o</sup> ]	Height [counts]	FWHM [2θ]	Rel. int. [%]
AMPS-g-TFC	26.27	3.39	10.72	0.23	4.35
	38.18	2.35	246.38	0.13	100.00
	44.40	2.04	183.76	0.09	74.58
MgSiO <sub>3</sub> NPs modified AMPS-g-TFC	10.28	8.60	0.66	0.23	0.16
	17.83	4.97	7.26	0.23	1.72
	18.37	4.82	5.79	0.23	1.38
	38.10	2.36	140.05	0.07	33.28
	44.43	2.03	420.83	0.09	100.00
	54.66	1.67	0.57	0.23	0.14

**Fig. 7** SEM images of *top* surface: **a** polysulfone support and **b** thin film composite membrane (TFC), **c** AMPS-g-TFC membrane, and **d** MgSiO<sub>3</sub> NPs modified AMMPS-g-TFC membrane

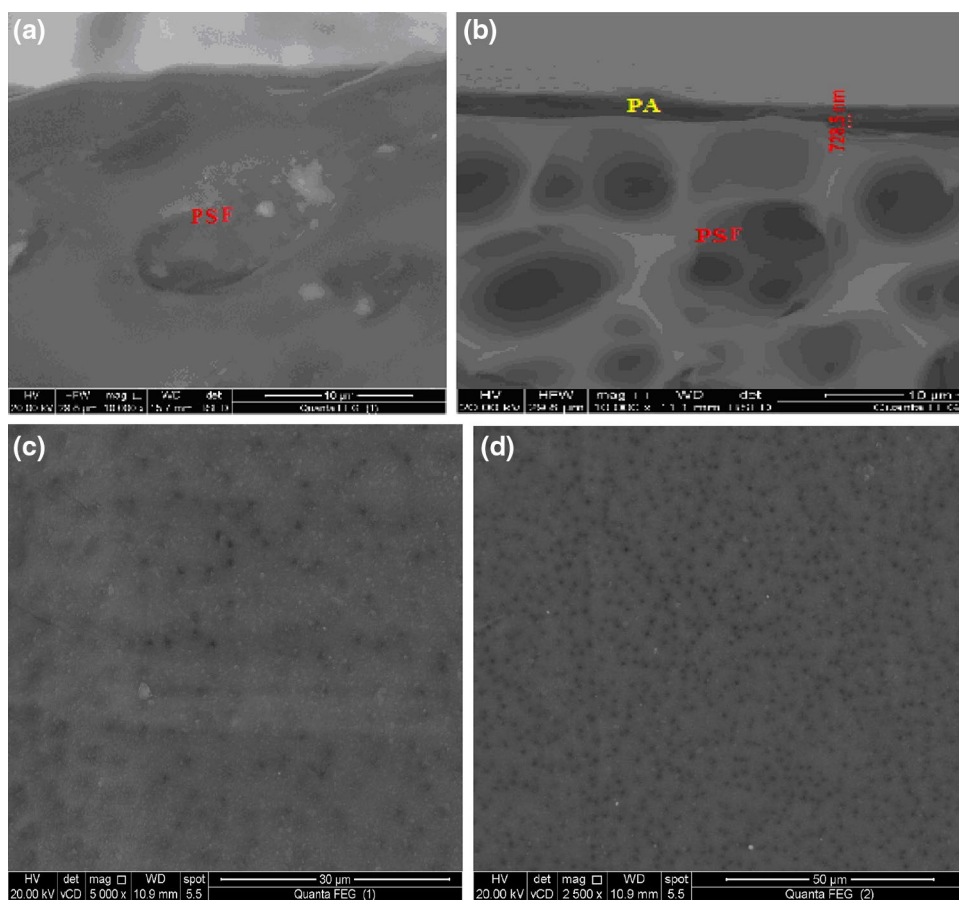
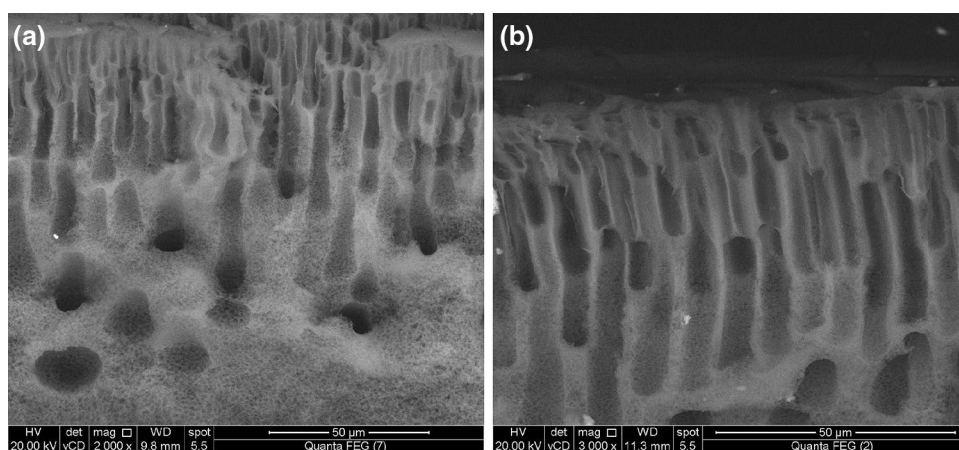


**Fig. 8** Cross-section SEM images of: **a** AMPS-g-TFC membrane and **b** MgSiO<sub>3</sub> NPs modified AMMPS-g-TFC membrane



### 3.4 Mechanical Properties of the Synthetic Membranes

To comprehension of the mechanical conjugation among the polymer pattern and attached MgSiO<sub>3</sub> NPs, the stress and strain characters of PSF, TFC, AMPS-g-TFC and MgSiO<sub>3</sub> NPs modified AMPS-TFC membranes have been presented in Fig. 9. Where AMPS-g-TFC and MgSiO<sub>3</sub>NPs modified AMPS-g-TFC membranes exhibit enhanced tensile strength under extreme physical operation conditions, also increase

the elongation break percentage additionally, raise Young's modulus grades remarkably when compared with pristine TFC membranes. this can be explained by; the bonding between the polyamide and the MgSiO<sub>3</sub>NPs-AMPS grafted monomer as illustrated by FTIR is energetically desirable, which favorable transfer the mechanical load from the polymer matrix to the grafted rigid nano-MgSiO<sub>3</sub> particles. Also, homogenous distribution and well dispersion of MgSiO<sub>3</sub> nanoparticles through AMPS monomer grafted to the TFC

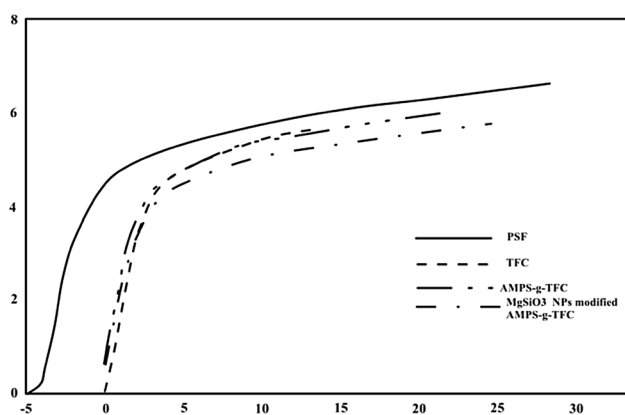


**Fig. 9** DMA curves show stress and strain of PSF support, thin film composite membrane (TFC), AMPS-g-TFC membrane, and MgSiO<sub>3</sub> NPs modified AMPS-g-TFC membrane

membrane matrix could transfer enough load through the interfacial and boundary shear stress and therefore the full intensity of the membrane can be responsible with more rigidity to the applied mechanical load which constantly transferred upon the MgSiO<sub>3</sub>NPs-AMPS grafted monomer prevented the progress of cracks through the polymer matrix [36]. So it is possible to conclude that homogeneous and well dispersed relative smaller particle size of MgSiO<sub>3</sub>NPs, as can be spotted in SEM analysis, also The added double bonding sites through the grafted AMPS grafted monomer ensure the efficiency absorbing of mechanical energy and distribute the external load hence increasing nanocomposite membrane mechanical properties [37].

### 3.5 Hydrophilicity of the Membranes

Contact angle examination is one of the basic parameters for determining membrane surface charges and hydrophilic/hydrophobic characters which have a great influence on membrane both water permeability and susceptibility for fouling [38]. While as contact angle becomes lower this means that the membrane surface turns to be more hydrophilic as the water particles have a great tendency to wet the surface layer. This, in turn, raises the membrane water flux [39]. Figure 10 demonstrates the contact edge ( $\theta$ ) estimations of PSF, TFC, AMPS-g-TFC and MgSiO<sub>3</sub> NPs modified AMPS-g-TFC membranes. From Fig. 10 the PSF substrate demonstrates contact angle equals to 72.8° this indicates weak membrane surface wettability with water and moderately hydrophobic properties. After interfacial polymerization, the hydrophilicity of TFC membrane was enhanced, and it diminished to 68.3° this demonstrated the PA layer was reasonably hydrophilic, with modification of the TFC membrane by monomer AMPS grafting, the contact angle achieved 62.1°. The low contact angle of the AMPS-g-TFC

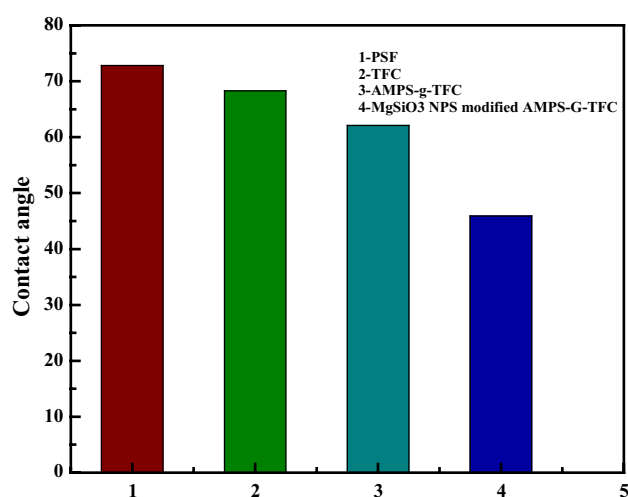


**Fig. 10** Contact angles results of the surface of PSF support, thin film composite membrane, AMPS-g-TFC membrane, and MgSiO<sub>3</sub> NPs modified AMPS-g-TFC membrane

layer demonstrated more hydrophilic properties indicated more hydrophilic properties because of the gatherings of polar and hydrophilic groups of sulfonic acids in the AMPS monomer structure. Moreover, MgSiO<sub>3</sub> NPs modified AMPS-g-TFC membrane exhibits the lowest contact angle which reached approximately 45.9° at 25 °C; confirm the excellent surface hydrophilicity owing to the still subsistence of free silicate species on membrane surfaces. Those free silicate groups act as a dynamic hydrophilic functional group on the membrane surface, which causes higher association in water and surface, through the favorable Si–OH forming groups. The considerable enlargement in membrane hydrophilicity produces increasing in the modified membrane permeability.

### 3.6 Membranes Thermal Behavior

Thermal performance of the fabricated polymer is an important property to evaluate the modification effects on a degradation behavior of different membranes. (TGA) as a common thermal analysis method was used to study the thermal stability of PSF, TFC, AMPS-g-TFC, and MgSiO<sub>3</sub> NPs modified AMPS-g-TFC membranes through a nitrogen gas environment and the results appeared in Fig. 11. It can be observed that both PSF and TFC membrane goes through thermal decomposition primary at 451.4–561.97 °C and 304.70–551.94 °C for PSF and TFC respectively, this could be regarded to the sulfonic group in chains of the polymer [40]. Also, another weight loss stage occurred above 729.9 and 760 °C is corresponding to the main polymer chain splitting as the presence of S=O group, which may be conjugated with H<sub>2</sub>O resulting in the formation of inter-molecular hydrogen bonds. As TFC membrane mainly constituted from

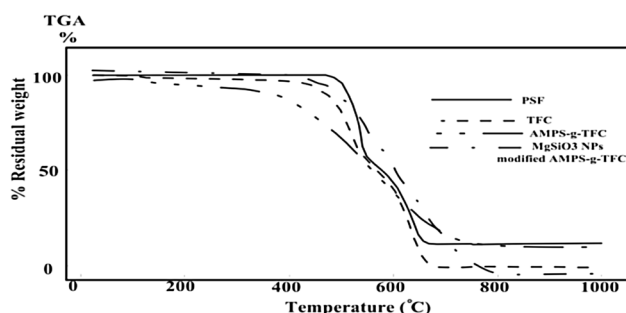


**Fig. 11** TGA curves of polysulfone support (PSF), thin film composite membrane (TFC), AMPS-g-TFC membrane, and MgSiO<sub>3</sub> NPs modified AMPS-g-TFC membrane

amide groups moreover aromatic rings, which are characterized by its resistance to change in temperature, so that the weight reduction in TFC layer happens over 760 °C is associated with the detachment of carbon molecules above 600 °C [41].

TGA diagram of AMPS-g-TFC membrane shows more thermal stability by comparing to the absolute TFC membrane, which possibly due to presences of more bonded amide and sulphonic groups in AMPS monomer. The TGA behavior of MgSiO<sub>3</sub> NPs modified AMPS-g-TFC membrane presented in Fig. 11, show that thermal decomposition was displaced to a greater temperature than AMPS-g-PATFC membrane. The initial weight loss, among 490–610 °C, which increased to more than 50 °C, this is basically because of the increase in binding water accompanied by the attachment of MgSiO<sub>3</sub>NPs which is confirmed by using FTIR test. Also, another weight loss, within 630–790 and 820 °C, may be attributed due to the elimination of, SO<sub>3</sub>, and SO<sub>2</sub> molecule from the grafted polymer [42]. These TGA results indicate that MgSiO<sub>3</sub> NPs incorporation remarkably reinforces the thermal resistance of the AMPS-g-TFC membrane.

### 3.7 Performance Evaluation

Membrane performance enhancement for desalination by surface coating with magnesium silicate nanoparticles using the free radical grafting technique and assessed the membrane performance including membrane flux of permeated water and salt rejection are the main target of this work. In this study, various parameters were studied such as the concentration of AMPS monomer, the concentration of MgSiO<sub>3</sub> NPs, grafting time and temperature to get the optimum condition necessary to prepare the best suitable MgSiO<sub>3</sub> NPs modified AMPS-g-TFC membrane for desalination of water which compared with pristine PA-TFC membrane which have 89.7% salt rejection and water flux 17.6 L m<sup>2</sup>h at water salinity 2000 ppm and at pressure 15 bar.

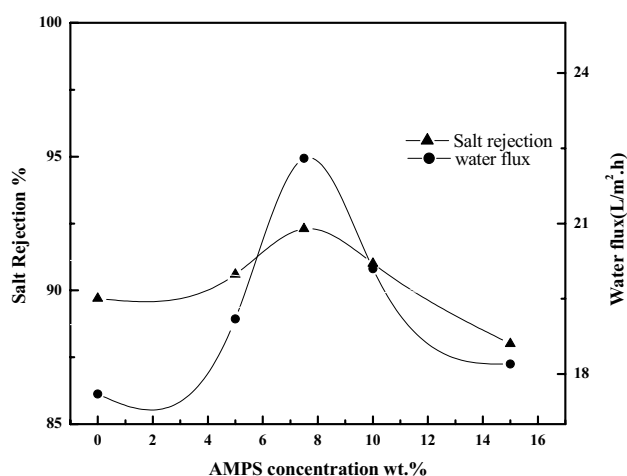


**Fig. 12** Effect of grafted AMPS monomer concentration on salt rejection and water flux of the resulting AMPS-g-TFC membrane testing with 2000 mg/L NaCl aqueous solution at 15 bar, 25 °C (after 60 min)

#### 3.7.1 The Concentration of Monomer AMPS and MgSiO<sub>3</sub> NPs

Figures 12 and 13 show permeate water flux and the salt rejection of prepared membranes with various concentrations of AMPS monomer, and MgSiO<sub>3</sub> NPs respectively. It is observed that both permeate water flux and salt rejection increases with nanomaterial concentration increasing. Then, for higher concentrations, it decreases; these results can be clarified as the increasing of coating layers on the membrane could reduce the permeation flux. Also, the reduction in the salt rejection may be due to some coating layers could minimize the surface charge due to the concealment, which then minimizes the salt rejection due to the Donnan effect phenomena [43]. The results reflect the existence of an optimum concentration of AMPS monomer and MgSiO<sub>3</sub> NPs.

#### 3.7.2 Grafting Time and Temperature

By over increasing in grafting time or curing temperature as in Figs. 14 and 15, membranes water flux, and salt rejection have been decreased, this may be due to The decreasing of the interchain hydrogen bonds as large amount of AMPS molecules were incorporated into aromatic polyamide chains, which may increase the polymer chain mobility, causing conformational alteration of aromatic polyamide chains. It might also create local destruction or compaction in the modified membrane surface and finally consequence in increased passing of both water and salt [44].

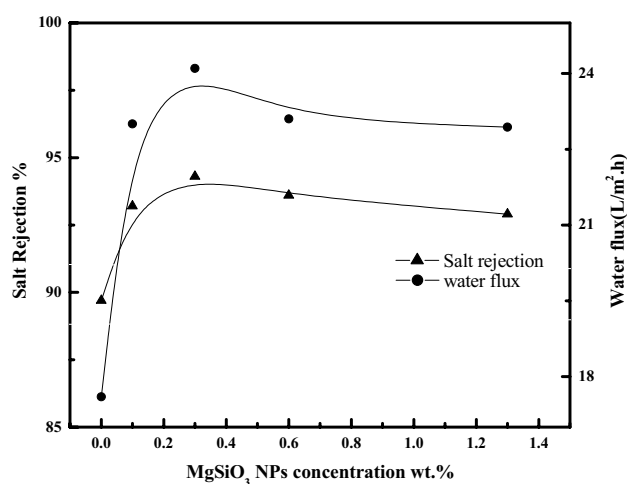


**Fig. 13** Effect of  $\text{MgSiO}_3$  NPs concentration on salt rejection and water flux of the resulting  $\text{MgSiO}_3$  NPs modified AMPS-g-TFC membrane testing with 2000 mg/L NaCl aqueous solution at 15 bar, 25 °C (after 60 min)

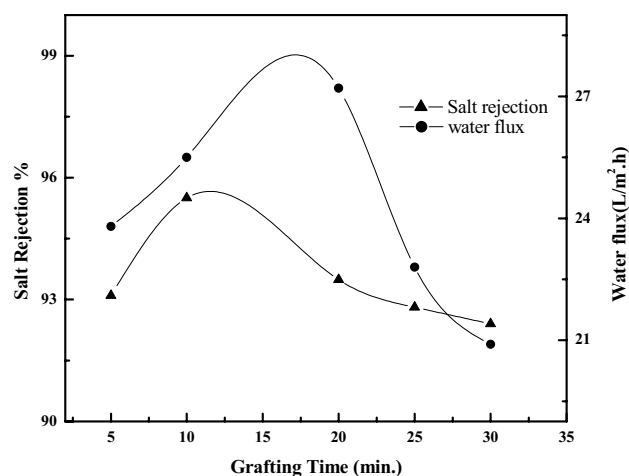


**Fig. 15** Effect of grafting time on salt rejection and water flux of the resulting  $\text{MgSiO}_3$  NPs modified AMPS-g-TFC membrane testing with 2000 mg/L NaCl aqueous solution at 15 bar, 25 °C (after 60 min.)

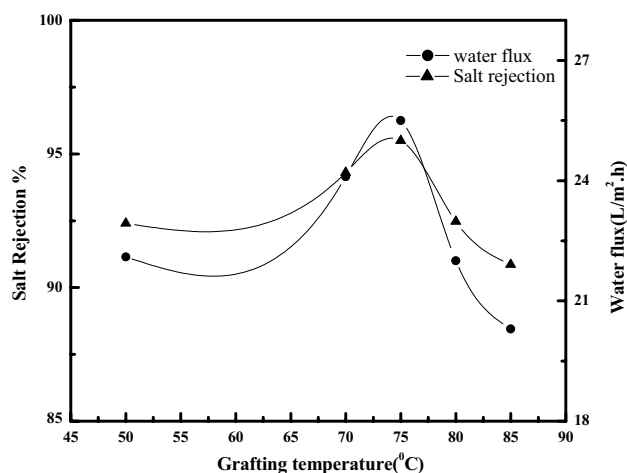


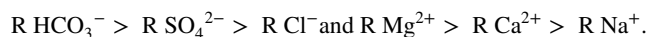
**Fig. 14** Effect of grafting temperature on salt rejection and water flux of the resulting  $\text{MgSiO}_3$  NPs modified AMPS-g-TFC membrane testing with 2000 mg/L NaCl aqueous solution at 15 bar, 25 °C (after 60 min)

### 3.8 Application of the Resulting $\text{MgSiO}_3$ NPs Modified AMPS-g-TFC Membrane on Sea Water and Different Ground Water Salinity

A seawater sample from a beach well located in Cleopatra region, Marsa Matrouh, and groundwater samples gathered from various sites on the northwestern coast of Egypt, have been applied as a water source to the RO pilot system utilizing the prepared flat sheets of  $\text{MgSiO}_3$  NPs modified AMPS-g-TFC membrane.

The different kind of feed water and the corresponding product water through the Lab. RO unit was investigated for

the major ion ingredients to define the performance of every membrane through different applied pressure, at a constant temperature of (25 °C), and also fixed flow rate about (5 L/min), a brief result of feed and product water analysis results are observed in Table 2. From results, the salt rejections of ( $\text{Mg}^{2+}$  and  $\text{SO}_4^{2-}$ ) divalent ions are greater than the rejection of ( $\text{Na}^+$  and  $\text{Cl}^-$ ) monovalent ions, where the retention for the divalent anions is fewer than cations ions. This can be demonstrated by the coefficients of mass transfer for divalent ions are lower than those for the monovalent ions and hence higher values for solute separations with respect to divalent ions [45]. Additionally, the degree of hydration which is a function of both size and charge/ being higher for small ions with a large charge, since there is a strong interaction of the solute ions with water molecules (ion–dipole influence) [46]. So that, the rejection of different ions is in the order:



By applying, different pressure on the prepared composite membranes of  $\text{MgSiO}_3$  NPs modified AMPS-g-TFC membrane with different water types as in Table 3 and Figs. 16 and 17 the results of both water flux and salt rejection increase gradually as an operating pressure increases, and by the further increase of the operation pressure, water flux increases dramatically comparing with increase in salt rejection. It can be clarified by the way that, permeate is directly corresponding to the networking pressure and the solute diffusion across the membrane [47, 48]. By analyzing the metal concentration in the permeate flux of the applicant water which applied on  $\text{MgSiO}_3$  NPs modified AMPS-g-TFC membrane, we observed that there is no release of both magnesium and silicon which confirms that,  $\text{MgSiO}_3$  NPs attached to thin film composite

**Table 2** Low brackish, high brackish groundwater and sea water characters before and after desalination process at 30 bar operation pressure

Analytical parameter (mg/L)	Feed water samples results			Product water results		
	Low brackish water	High brackish water	Sea water	Low brackish water	High brackish water	Sea water
TDS	5650.0	10660.0	40000.0	226.0	426.0	1100.0
Na <sup>+</sup>	1057.0	1670.0	11050.0	60.0	107.0	185.0
K <sup>+</sup>	17.0	24.0	516.0	3.3	3.0	4.6
Mg <sup>2+</sup>	244.0	560.0	1880.0	5.5	4.2	10.0
Ca <sup>2+</sup>	630.0	1180.0	520.0	16.0	28.0	13.0
HCO <sub>3</sub> <sup>-</sup>	50.0	106.0	138.0	3.0	4.0	3.5
SO <sub>4</sub> <sup>2-</sup>	250.0	510.0	2890.0	14.0	18.0	80.0
Cl <sup>-</sup>	2980.0	5800.0	20850.0	118.0	230.0	520.0

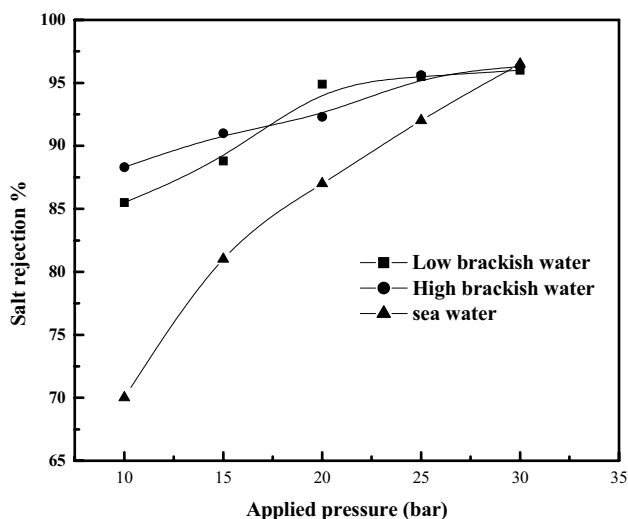


**Fig. 16** Effect of operating pressure on salt rejection of the MgSiO<sub>3</sub> NPs modified AMPS-g-TFC membrane testing low brackish, high brackish groundwater and sea water

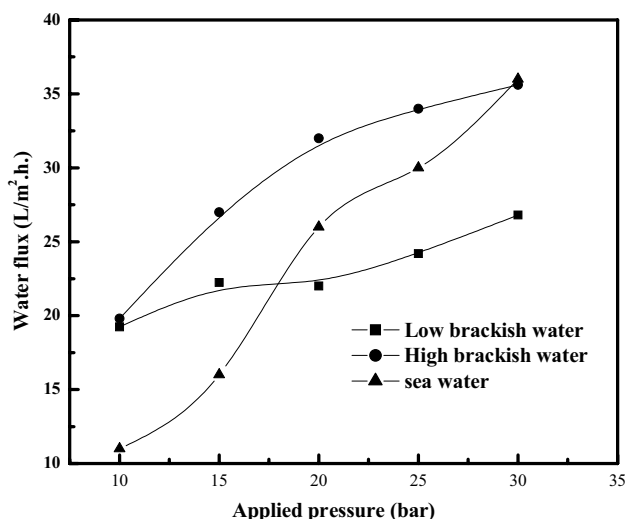


**Fig. 17** Effect of operating pressure on water flux of the MgSiO<sub>3</sub> NPs modified AMPS-g-TFC membrane testing low brackish, high brackish groundwater and sea water

membrane via a chemical bond. Application results demonstrate that MgSiO<sub>3</sub> NPs modified AMPS-g-TFC membrane show high desalination performance under different operating conditions and can be used as an applicable good modification for PA TFC membrane with modified properties.

#### 4 Conclusions

MgSiO<sub>3</sub> NPs were attached to the surface of TFC membrane with AMPS monomer as a bridging agent via free radical grafting technique. MgSiO<sub>3</sub> NPs modified AMPS-g-TFC membrane showed superior mechanical and thermal stability

**Table 3** Comparison between salt rejection and water flux of different types of water low brackish, high brackish groundwater and seawater samples at different operation pressure

Pressure (bar)	Low brackish water		High brackish water		Sea water	
	Salt rejection %	Water flux (L/m <sup>2</sup> h)	Salt rejection (%)	Water flux (L/m <sup>2</sup> h)	Salt rejection (%)	Water flux (L/m <sup>2</sup> h)
10	85.50	19.25	88.30	19.80	70.00	11.00
15	88.80	22.25	91.00	27.00	81.00	16.00
20	94.90	22.00	92.30	32.00	87.00	26.00
25	95.50	24.20	95.60	34.00	92.00	30.00
30	96.00	26.80	96.30	35.60	96.50	36.00

while has a high hydrophilic surface, as the contact angle with water reached ( $\sim 45.9^\circ$ ). Microscopic and morphology of modified nanocomposite membrane also examined using FT-IR, XRD, and SEM. Furthermore, water flux and a salt rejection for the resulted membranes were assessed, where performance of the newly modified membrane gave about  $28.2 \text{ L m}^2 \text{ h}$  as a permeate water flux and a salt rejection of  $\geq 95.5\%$  was obtained for a saline water (2000 ppm of NaCl) at an applied pressure about 15 bars with a 32% increase in water flux comparing to the pristine TFC membrane. This study demonstrates that the  $\text{MgSiO}_3$  NPs modified AMPS-g-TFC membrane could remarkably enhance selectivity, water permeability and surface hydrophilic characters of membranes for a different application of desalination and water filtration. These promising features of the modified membrane are possible to have a great impact on desalination process economics in terms of the capital and running costs.

**Acknowledgements** It is a pleasure to acknowledge the financial support provided by the Science and Technological Development Fund (STDF) in Egypt through Grant 5240 (Egyptian Desalination Research Center of Excellence, EDRC).

## References

- (UNEP). Annual Report, from [https://na.unep.net/geas/getUNEP-PageWithArticleIDScript.php?article\\_id=76](https://na.unep.net/geas/getUNEP-PageWithArticleIDScript.php?article_id=76) January 2012
- D.W. Seckler, U. Amarasinghe, D. Molden, R. de Silva, R. Baker, *Research report world water demand and supply 1990 to 2025*, (Srilanka, Colombo, 1998)
- MWRI, *Water scarcity in Egypt*, (MWRI, Pittsburgh, 2014)
- M.L. Parry, *Impacts, adaptation and vulnerability, in climate change 2007*, Cambridge University Press, Cambridge (2007)
- IDA, *IDA desalination yearbook 2015–2016.*, (Media Analytics Ltd. ed, Oxford. 2015)
- GWII, Market profile. In: *IDA Desalination Yearbook 2015–2016.* (Media Analytics Ltd. ed, Oxford. 2015)
- K.P. Lee, T.C. Arnot, D. Mattia, *J. Appl. Polym. Sci.* **370**(1), 1–22 (2011)
- B. Peñate, L. García-Rodríguez, *Desalination* **284**, 1–8 (2012)
- G.P. Sean, N.P. Cheer, A.F. Ismail, *Membrane fabrication*, N. Hilal, A. F. Ismail, C. Wright, (CRC Press, Boca Raton, 2015), p. 489
- J.B. Li, J.W. Zhu, M.J. Zheng, *J. Appl. Polym. Sci.* **103**, 3623 (2007)
- R.D. Noble, D. Richard, *J. Appl. Polym. Sci.* **378**, 393–397 (2011)
- J.M. Arsuaga, A. Sotto, G. del Rosario, A. Martínez, S. Molina, S.B. Teli, J. de Abajo, *J. Appl. Polym. Sci.* **428**, 131–141 (2013)
- A. Zehhaf, A. Benyoucef, C. Quijada, S. Taleb, E. Morallo'n, *Int. J. Environ. Sci. Technol.* **12**, 595–602 (2015)
- S. Kango, S. Kalia, A. Celli, J. Njuguna, Y. Habibi, R. Kumar, *Prog. Polym. Sci.* **38**(8), 1232–1261 (2013)
- S.H. Kim, S.Y. Kwak, T. Suzuki, *Environ. Sci. Technol.* **39**(6), 1764–1770 (2005)
- M. Ali, Y.H. Kotp, I.M. El-Naggar, *Desalination* **259**(1), 228–234 (2010)
- Y.H. Kotp, *Separat. Sci. Technol.* **52**(4), 657–670 (2017)
- M. Mekhloufi, A. Zehhaf, A. Benyoucef, C. Quijada, E. Morallon, *Environ. Monit. Assess.* **185**, 10365–10375 (2013)
- G. Socrates, *Infrared characteristic frequencies*, 2nd edn (Wiley, Hoboken, 1994).
- Y.N. Kwon, C.Y. Tang, J.O. Leckie, *J. Appl. Polym. Sci.* **102**(6), 5895–5902 (2006)
- H.S. Lee, S.J. Im, J.H. Kim, H.J. Kim, J.P. Kim, B.R. Min, *Desalination* **219**(1), 48–56 (2008)
- S. Sridhar, B. Smitha, T.M. Aminabhavi, *Separat. Purific. Rev.* **2**, 36 (2007)
- C.N.R. Rao, *Chemical applications of infrared spectroscopy*. (Academic Press, New York, 1963)
- H. Song, S.F. Zhang, X.C. Ma, D.Z. Wang, J.Z. Yang, *Carbohydr. Polym.* **69**(1), 189–195 (2007)
- V. Azmeera, P. Adhikary, S. Krishnamoorthi, *Int. J. Carbohydr. Chem.* (2012)
- J. Dechant, R. Danz, W. Kimmer, R. Schmolke, *Ultraspektroskopische Untersuchungen an Polymeren*. (Akad. Verlag, Berlin, 1972)
- N.T. Tran, T. Min, A.K. Franz, *Chem. A Eur. J.* **17**(36), 9897–9900 (2011)
- B.J. de Aragão, Y. Messaddeq, *J. Brazil. Chem. Soc.* **19**(8), 1582–1594 (2008)
- D. Cassimatis, J.P. Bonnin, T. Theophanides, *Can. J. Chem.* **48**(24), 3773–3781 (1970)
- C.S. Riccardi, R.C. Lima, M.L. Dos Santos, P.R. Bueno, J.A. Varela, E. Longo, *Solid State Ion* **180**, 288–291 (2009)
- R. Padmavathi, R. Karthikumar, D. Sangeetha, *Electrochim. Acta*, **71**, 283–293 (2012)
- S.K. Yong, W.L. Sang, Y.K. Un, S.S. Jyong, *J. Membr. Sci.* **51**, 215–226 (1990)
- L. Li, S. Zhang, X. Zhang, G. Zheng, *J. Membr. Sci.* **289**(1), 258–267 (2007)
- B. Deng, C. Ding, J. Yin, *J. Chem. Proc. Eng.* **1**, 1–8 (2014)
- S.Y. Kwak, M.O. Yeom, I.J. Roh, D.Y. Kim, J.J. Kim, *J. Membr. Sci.* **132**(2), 183–191 (1997)
- C. Wei, K. Cho, D. Srivastava, *MRS Proceedings*, (Cambridge University Press, Cambridge, 2001)
- J. Li, J. Suo, R. Deng, *J. Reinf. Plasti. Compos.* **29**(4), 618–629 (2010)
- W.R.F., *Evaluation of Membrane Characterization* (2012)
- S.S. Shenvi, S.A. Rashid, A.F. Ismail, M.A. Kassim, A.M. Isloor, *Desalination* **315**, 135–141 (2013)
- Y.F. Liu, Q.C. Yu, Y.H. Wu, *Electrochim. Acta* **52**(28), 8133–8137 (2007)
- S. Villar-Rodil, J.I. Paredes, A. Martinez-Alonso, J.M.D. Tascon, *Chem. Mater.* **13**, 4297–4304 (2001)
- A. Srivastava, P. Mandal, R. Kumar, *Int. J. Biol. Macromol.* **87**, 101–113 (2016)
- G.R. Xu, J.N. Wang, C.J. Li, *Desalination* **328**, 83–100 (2013)
- X. Wei, Z. Wang, Z. Zhang, J. Wang, S. Wang, *J. Membr. Sci.* **351**(1), 69–74 (2010)
- M. Khayet, J.I. Mengual, *Desalination*, **168**, 373–381 (2004)
- S.M. Ghiu, R.P. Carnahan, M. Barger, *Desalination* **157**(1), 385–393 (2003)
- Y. Zhou, S. Yu, M. Liu, C. Gao, *Desalination* **180**, 189–196 (2005)
- M. Liu, D. Wu, S. Yu, C. Gao, *J. Membr. Sci.* **326**, 64–75 (2009)